

# SYNTHESIS AND CHARACTERISATION OF NANOCRYSTALLINE ZrN PVD COATINGS ON AISI 430 STAINLESS STEEL

A.V. Taran<sup>1</sup>, I.E. Garkusha<sup>1,4</sup>, V.S. Taran<sup>1</sup>, R.M. Muratov<sup>1</sup>, T.S. Skoblo<sup>2</sup>, S.P. Romaniuk<sup>2</sup>, V.V. Starikov<sup>3</sup>, A.A. Baturin<sup>3</sup>

<sup>1</sup>National Science Center “Kharkov Institute of Physics and Technology”,  
Institute of Plasma Physics, Kharkiv, Ukraine;

<sup>2</sup>National Technical University of Agriculture, Kharkiv, Ukraine;

<sup>3</sup>National Technical University “Kharkov Polytechnic Institute”, Kharkiv, Ukraine;

<sup>4</sup>V.N. Karazin Kharkiv National University, Kharkiv, Ukraine

Email: avtaran@ukr.net

The nanocrystalline films of zirconium nitride have been synthesized using ion-plasma vacuum-arc deposition technique in combination with high-frequency discharge (RF) on AISI 430 stainless steel at 150°C. Structure examinations X-ray fluorescent analysis (XRF), X-ray diffraction analysis (XRD), scanning electron microscopy (SEM) with microanalysis (EDS), and transmission electron microscopy (TEM), nanoindentation method – were performed to study phase and chemical composition, surface morphology, microstructure and nanohardness of coatings. The developed technology provided low-temperature coatings synthesis, minimized discharge breakdown decreasing formation of macroparticles (MPs) and allowed to deposit ZrN coatings with hardness variation 26.6...31.5 GPa. It was revealed that ZrN single-phase coatings of cubic modification with finecrystalline grains of 20 nm in size were formed.

PACS: 52.77.-j; 81.20.-n

## INTRODUCTION

Zirconium nitride (ZrN) ceramic with cubic structure has high wear, fatigue and corrosion resistance properties and is widely used as hard, refractory and bioinert coating in industry and medicine [1-4]. Crystal structure and mechanical properties of ZrN are similar to TiN, but ZrN lattice parameter exceeds TiN one (ZrN,  $a = 4.58 \text{ \AA}$  and TiN,  $a = 4.24 \text{ \AA}$ ). According to Zr-N phase diagram there are stoichiometric ZrN and non-stoichiometric metastable  $Zr_2N$ ,  $ZrN_2$ ,  $Zr_3N_4$  and  $Zr_4N_3$  phases [5]. Hardness and elastic modulus of the ZrN coating is around 25 and 420 GPa respectively [6-11]. Wear test results indicated that ZrN is similar to titanium nitride in conventional metal cutting applications, but outperforms TiN by a factor of two when cutting titanium and aluminum alloys [12].

ZrN thin films have been synthesized by various CVD and PVD deposition methods [13, 14]. It is well known that PVD technology modifies the surface properties of tools without changing the undercoating material properties and biomechanical functionality. Plasma based PVD coatings have favorable residual stresses, higher density and better adhesion compared to other techniques. macroparticles. The utilization of vacuum-arc evaporation with RF discharge allows applying coatings onto dielectrics and termoliable instrument at low temperature decreasing the amount of macroparticles emitted from plasma flow.

In the present paper ZrN coatings were obtained on AISI 430 stainless steel substrates using vacuum-arc deposition technique with high-frequency discharge regime (RF) at 150°C. Special attention was paid to functional properties of the obtained coatings dependent on the microstructure (grain size, phase composition, nanohardness) to settle the correlation between structure-phase conditions and mechanical properties of the coatings.

ISSN 1562-6016. BAHT. 2019. №1(119)

## 1. EXPERIMENTAL SETUP

ZrN coatings were synthesized using vacuum-arc method with RF discharge in Bulat-6 type device [15-18]. Bias potential was applied to the substrate from RF generator, which produced impulses of oscillations at 5 MHz frequency. Chemically pure zirconium (99.999) was used as a cathode material. Nitrogen 99.999% purity was used as an active gas. Polished stainless steel samples (AISI 430) of  $25 \times 25 \times 3 \text{ mm}$  size were used as the substrate material (roughness  $R_a \approx 0.09 \text{ \mu m}$ ). Chemical composition of AISI 430 according to XRF data is presented in Table 1.

Table 1

Chemical composition of AISI 430 SS

C	Mn	P	S	Si	Cr	Fe
0.12	1.0	0.035	0.03	1.0	17.0	81

Before deposition, the substrates were cleaned in an ultrasonic bath for 10 min. The surface cleaning in RF discharge was carried out in argon plasma for substrate degreasing and removing impurities during 15 min ( $U_{\text{bias}} = 1000 \text{ V}$ ,  $P(\text{Ar}) = 6 \times 10^{-1} \text{ Pa}$ ). The Zr buffer layer of 20 nm thickness was deposited before the nitride coatings to improve coating adhesion. It was used  $I_{\text{arc}} = 110 \text{ A}$ ,  $U_{\text{bias}}^{\text{RF}} = -200 \text{ V}$ , base pressure  $P = 5 \times 10^{-4} \text{ Pa}$  and deposition time 25 min.

The surface topography was studied using JEOL JSM-6390LV scanning electron microscope (SEM) with an accelerating voltage of 20 kV, chemical composition was examined using EDS analysis.

The microstructure and phase composition were investigated by methods of transmission electron microscopy (TEM) using EMV-100L electron microscope at accelerating voltage of 100 kV. The ZrN coatings of 70 nm thickness were synthesized on (001)

KCl chipped crystals for transmission electron microscopy using the same deposition parameters.

Energy-dispersive spectrometer SPRUT-K (AO Ukrrentgen, Ukraine) was used for X-ray fluorescent analysis and was equipped with Si (Li) X-100 detector (Amptek, USA) in the arrangement with a Si and KCl secondary target. An X-ray tube BS-22 with shooting-through type Ag anode was applied. The tube regime: U = 35 kV, I = 250 A, and exposure time 300 s. Film thickness was determined by XRF examinations and average film thickness was 1.67  $\mu\text{m}$ .

X-ray diffraction (XRD) analysis were performed using DRON-3M device, under Cu-K $\alpha$  radiation, monohromated by (002) HOPG in diffracted beam. The XRD line scans were performed in  $\theta$ -2 $\theta$  scanning mode where the incident angle  $\theta$  and diffracted angle 2 $\theta$  are scanned simultaneously.

The nanohardness was measured by Nanoindenter G200 (USA). The loading and unloading rates of the nanoindentation were 10 mN/min. Samples were tested to a depth of 500 nm. The distance between prints were 15  $\mu\text{m}$  and for each sample was made 7 prints.

## 2. RESULTS AND DISCUSSION

### 2.1. STRUCTURE, CHEMICAL AND PHASE COMPOSITION

A typical XRD pattern of ZrN coating obtained in RF regime is presented in Fig.1.

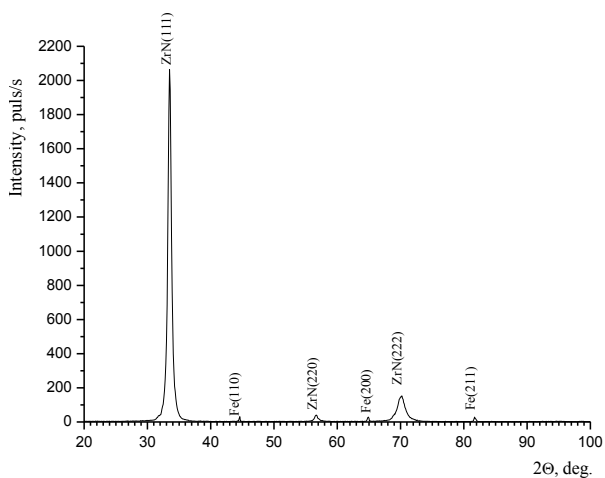


Fig. 1. XRD spectra of ZrN coating

All angles of diffraction peaks with (111), (222), and (220) main reflections were indexed as ZrN phase with a crystal structure of B1 NaCl cubic lattice type (according to JCPDS 35...0753,  $a = 0.4577$  nm lattice constant). The high intensity of the ZrN (111) Bragg peak, indicates that the ZrN grains grow with the [111] preferred orientation perpendicular to the growth plane. According to literature data, for transition nitrides with NaCl-type lattice, which belong to octahedral structures, periodic alternation of atomic layers fully occupied with only metal and non-metal (nitrogen) atoms took place along [111] direction. Such arrangement of the layers corresponds to the lowest surface free energy of the system and is the most frequently encountered case,

especially with low stresses developing in the condensate and at the initial stages of film growth.

The [111] texture was also monitored for various types of films (TiN, CrN, TiAlN, TiCN) deposited by cathodic arc technique. The presence of highly ionized plasma also favors the film growth in the most densely packed direction.

The width of XRD peaks indicated finocrystalline structure with the average grain size of 15...20 nm. It was reported that the high-frequency technique leads to smaller average crystallite size in comparison with the standard PVD mode due to higher density of nuclei's of crystal during its formation. The microdeformation of crystallites was also smaller at using of the RF method.

The XRD data has good correlation with TEM investigations. The electron-microscopic image and electron-diffraction pattern of ZrN film grown on (001) KCl are shown in Fig. 2,a,b.

All electron-diffraction lines were indexed as ZrN phase with *bcc* lattice having stoichiometric composition. No additional phases have been revealed. The obtained results are summarized in Table 2. The average grain size was 0.02  $\mu\text{m}$ .

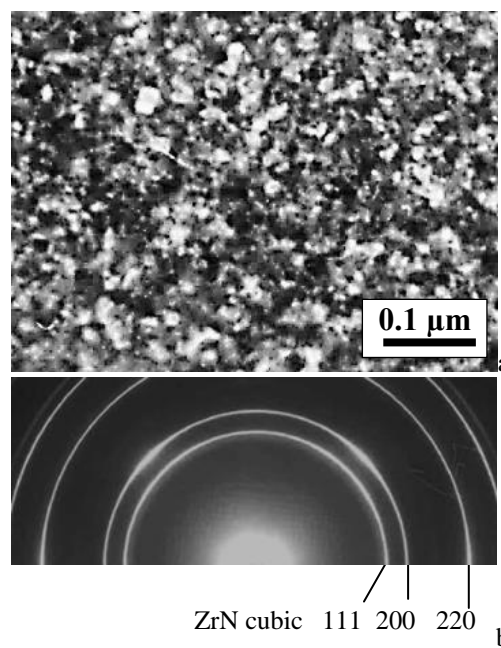


Fig. 2. TEM image (a), electron diffraction pattern (b) of ZrN

Table 2  
Interplanar distances of ZrN coating on (001) KCl

ZrN PDF (35-0573) d, Å Cubic	ZrN d, Å	I, %	h,k,l
2.64	2.63	100	(111)
2.29	2.27	74	(200)
1.61	1.59	36	(220)
1.38	1.36	24	(311)
1.32	1.32	9	(222)
1.14	1.15	2	(400)

The light optical microscopy images of the initial surface and deposited ZrN coating are presented in Fig. 3.

The surface morphology and chemical composition heterogeneity of ZrN coatings was also examined using scanning electron microscope JEOL JSM-6390LV, equipped with EDS. (Figs. 4, 5). The surface is rather smooth having a small number of macrodefects identified as drops from the cathode material. (Fig. 6,a-c). The size of macroparticles does not exceed 4  $\mu\text{m}$ . In accordance with energy-dispersive X-ray analysis the integral chemical composition was: Zr – 34.50 at.%, N – 38.86 at.%, O – 12.93 at.%, C – 13.22 at.%. (see Fig. 5,d).

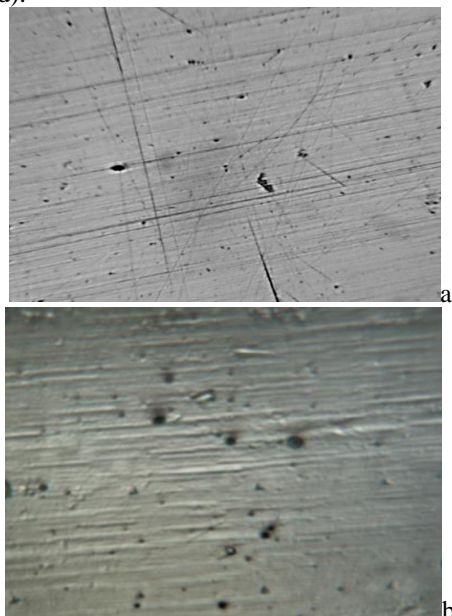


Fig. 3. Light optical microscopy images of the initial surface at  $\times 160$  (a), and ZrN coating at  $\times 300$  magnifications (b)

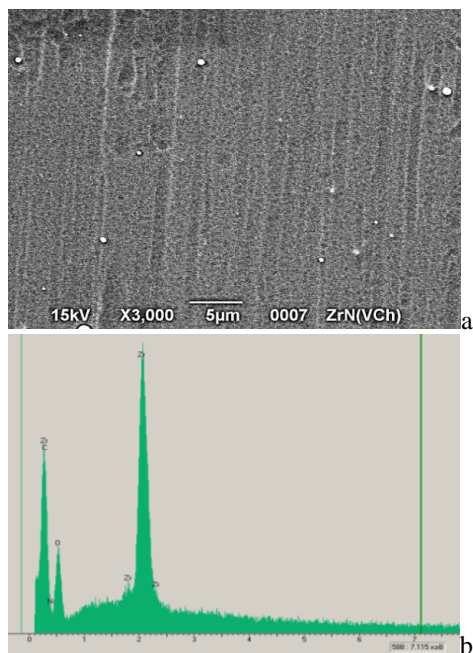


Fig. 4. Surface morphology (a) and (b) EDS spectra of ZrN coating

The presence of small quantity of oxygen and carbon is due to residual gas incorporated in the chamber walls and contamination during sample handling in open atmosphere before the composition analysis. Using

thermionic emission, it was monitored homogeneous distribution of selected chemical components on the surface (see Fig. 5,d). EDS microanalysis taken from four local areas is presented in Table 3.

Table 3  
Chemical composition from local selected areas (see Fig. 5,d) (EDS)

Element	Conc.	Intensity	wt.%	at.%
C	0.42	0.7480	3.89	13.22
N	0.29	0.1461	13.33	38.86
O	0.36	0.4829	5.07	12.93
Fe	0.09	0.9833	0.66	0.48
Zr	10.54	0.9330	77.06	34.50

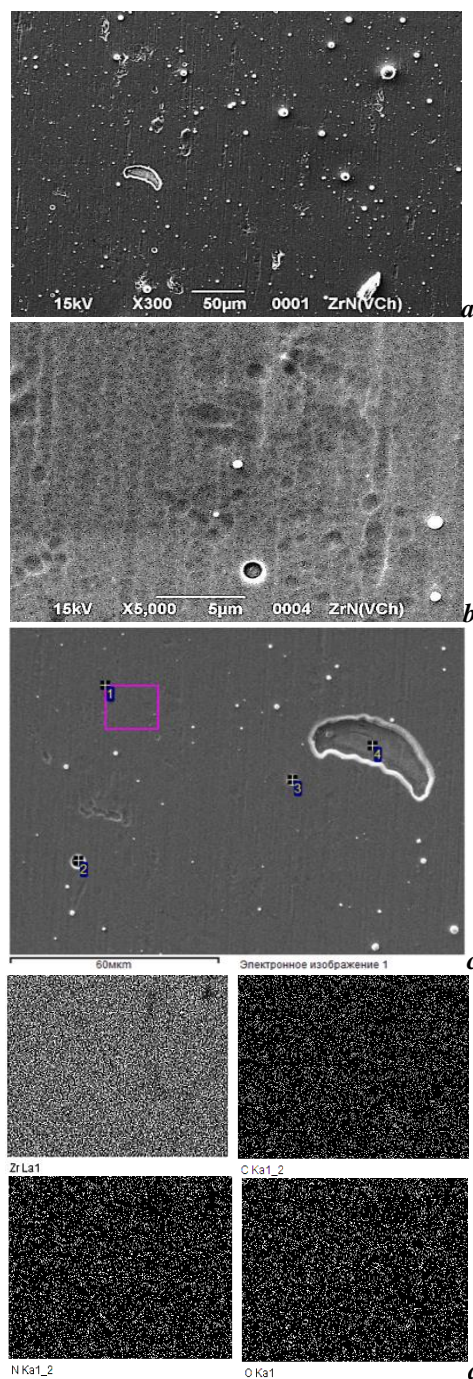


Fig. 5. SEM images (a-c) and homogeneous distribution of selected elements on the surface (d)

## 2.2. MECHANICAL PROPERTIES

The microhardness of the coating strongly depends on structural parameters such as crystallographic orientation, microstress, and crystallite size. One of the main characteristics of the material is the ratio of its hardness to the elastic modulus  $H/E$ , called plasticity index. The ratio  $H^3/E^{*2}$  (where  $E^* = E/(1 - \mu^2)$  – the effective elastic modulus;  $\mu$  – Poisson's ratio) is also qualitative comparative characteristic of the plastic deformation resistance. To increase the plastic deformation resistance it is required to strive for the lowest possible elastic modulus at high hardness which, in particular, takes place at grain sizes of less than 10 nm. In general, the low module is good, because it allows distributing load within a wide area.

Table 4  
Mechanical properties of AISI 430 and ZrN

	AISI 430			ZrN coating		
	E, GPa	H, GPa	H/E	E, GPa	H, GPa	H/E
1	204.496	3.727	0.018	336.309	31.071	0.092
2	184.049	4.084	0.021	333.475	31.576	0.094
3	203.588	3.872	0.019	288.604	26.11	0.090
4	205.773	3.99	0.019	302.027	26.635	0.088
5	198.272	3.61	0.018	316.364	29.188	0.092
6	202.134	4.559	0.022	331.657	29.14	0.087
7	209.751	3.8	0.018	337.236	32.047	0.095
	<b>201.151</b>	<b>4.092</b>	<b>0.02</b>	<b>320.81</b>	<b>29.395</b>	<b>0.091</b>

The effective elastic modulus  $E^*$ , the shear modulus  $G$ , yield stress point  $\sigma_T$  and coefficient of resistance to plastic deformation  $H^3/E^{*2}$  were determined using model equations. The shear modulus ( $G$ ) and yield stress ( $\sigma_T$ ) are defined as  $G = E / 2 \times (1 + \mu)$ ;  $\sigma_T = H\mu / 3$ .

The nanoindentation diagrams for ZrN coating are presented in Fig. 6. The results of  $H$  and  $E$  values for 7 prints are summarized in Tab.4. The  $G$ ,  $\sigma_T$ ,  $H^3/E^{*2}$  parameters were measured only for average  $H$  and  $E$  values and are presented in Table 5.

Table 5  
 $G$ ,  $\sigma_T$ ,  $H^3/E^{*2}$  parameters of AISI 430 and ZrN coating based on  $H$  and  $E$  average values

Sample	H [GPa]	E [GPa]	G [GPa]	$\sigma_T$ [MPa]	$H^3/E^{*2}$
AISI 430	4	204	62	133	0.0014
AISI 430/ZrN	29	320	121	966	0.05

According to nanoindentation tests, ZrN coating has much higher elastic properties than initial stainless steel. The average value of nanoindentation hardness for stainless steel was 4.09 GPa, and it reached 29.39 GPa for the ZrN coated sample. The average value of elastic modulus for the ZrN was 320.81 GPa, whereas without the coating it comprised 201.151 GPa with a data spread of 9.54 %. As it is seen from Table 5 that with increase of the ratio

$H/E$  decreases plasticity of material and increasing of its relative hardness.

The high hardness of the coatings can be associated with an improvement of homogeneity of ZrN coatings on the one hand and on the other, the hardness growth can be related to the grinding of the grain structure (according to Hall-Petch rule) by ion bombardment upon application high-voltage RF pulses to the substrate during the deposition process.

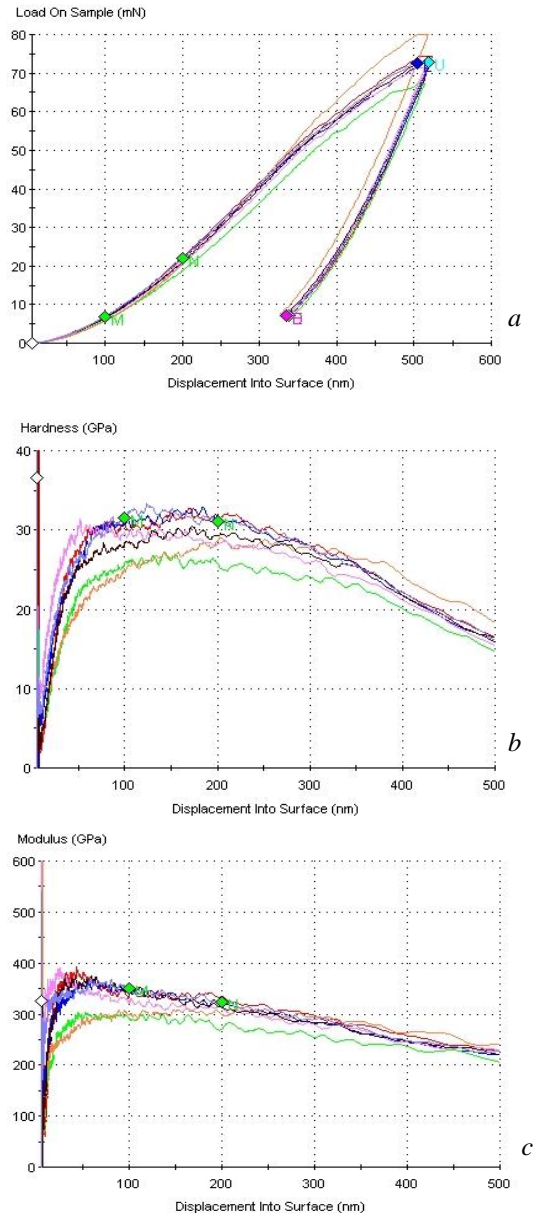


Fig. 6. Nanoindentation diagrams for the ZrN coating; load-unload diagram (a), nanohardness (b), elastic modulus (c)

## CONCLUSIONS

Zirconium nitride coatings have been synthesized using ion-plasma vacuum-arc deposition technique in combination with high-frequency discharge (RF) on AISI 430 stainless steel at 150°C.

The proposed technology allowed minimizing the amount of macroparticles providing low temperature deposition.

It was revealed that nanocrystalline ZrN single-phase coatings of cubic modification with finecrystalline grains of 20 nm in size were formed.

The average values of nanohardness and elastic modulus of ZrN were 29.39 and 320.81 GPa, respectively.

#### REFERENCES

1. W.J. Chou, C.H. Sun, G.P. Yu // *J. Mater. Chem. Phys.* 2003, v. 82, p. 228-233.
2. Mitsuo, T. Mori, Y. Setsuwhar, S. Miyake, T. Aizawa // *Inst. Meth.* 2003, v. B 206, p. 366-370.
3. M.M. Larijani et al. // *J. Cryst. Res. Technol.* 2011, v. 46(4), p. 351-356.
4. M. Banerjee et al. // *J. Crystal Growth and Design.* 2012, v. 12(10), p. 5079-5089.
5. Y. Dong, W. Zhao, Y. Li, G. Li // *J. Appl. Surf. Sci.* 2000, v. 252, p. 5057-5062.
6. M. Nose, W.A. Chiou, M. Zhou, T. Mae, M. Meshii // *J. Vac. Sci. Technol.* 2002, v. 20, p. 823-830.
7. P.C. Johnson, H. Randhawa // *J. Surface and Coating Technology.* 1987, v. 33, p. 53-62.
8. X. Liu, P.K. Chu, C. Ding // *J. Mater Sci Eng.* 2004, v. 47, p. 49-121.

9. D.J. Blackwood // *In Shreir's Corrosion / 4th ed.*; Elsevier. 2010, v. 2, p. 1308-1322.
10. M.A. Rizzo et al. // *J. Thin Solid Films*, 2006, v. 515, p. 1486-1490.
11. L. Rogström et al. // *J. Thin Solid Films.* 2010, v. 519, p. 694-699.
12. L. Pichon, A. Straboni, T. Girardeau, M. Droue // *J. Appl. Phys.* 2000, v. 87, p. 925-930.
13. M.H. Shiao, Z.C. Chang, F.S. Shieu // *Journal of the Electro. Soc.* 2003, v.150, p. 320-324.
14. C Liu, A. Leyland, A. Matthews // *Corr. Sci.* 2003, v. 45, p. 1243-1256.
15. T.S. Skoblo, S.P. Romaniuk, A.I. Sidashenko, I.E. Garkusha, A.V. Taran, et al. // *J. Adv. Microsc. Res.* 2018, v. 13, p. 333-338.
16. A.V.Taran I.E. Garkusha, V.S. Taran, et al. // *J. Adv. Microsc. Res.* 2018, v. 13, p. 313-319.
17. V. Tereshin, V. Taran, et al // *J. Vacuum.* 2003, v. 73, p. 555-559.
18. V. Gasilin, O. Svets, V. Taran, et al. // *J Appl. Plasma Science.* 2005, v. 13, p. 87-93.

Article received 22.09.2018

#### СИНТЕЗ И ИССЛЕДОВАНИЕ НАНОКРИСТАЛЛИЧЕСКИХ ПОКРЫТИЙ ZrN, ПОЛУЧЕННЫХ ВАКУУМНО-ДУГОВЫМ МЕТОДОМ НА НЕРЖАВЕЮЩЕЙ СТАЛИ AISI 430

*А.В. Таран, И.Е. Гаркуша, В.С. Таран, Р.М. Муратов, Т.С. Скобло, С.П. Романюк, В.В. Стариков, О.А. Батулин*

Нанокристаллические пленки нитрида циркония были синтезированы вакуумно-дуговым методом с применением высокочастотного разряда (ВЧ) на поверхности нержавеющей стали марки AISI 430 при 150°C. Для изучения фазового и химического составов, морфологии поверхности, микроструктуры и нанотвердости покрытий применялись рентгенофлуоресцентный (XRF) и рентгеноструктурный (XRD) анализы, сканирующая электронная микроскопия (SEM) с микроанализом (EDS) и просвечивающая электронная микроскопия (TEM). Разработанная технология обеспечивает низкотемпературный синтез покрытий, уменьшая образование макрочастиц, а также позволяет осаждать покрытия ZrN с твердостью 26,6...31,5 ГПа. Установлено образование однофазных поликристаллических пленок ZrN кубической модификации с размером зерен 20 нм.

#### СИНТЕЗ І ДОСЛІДЖЕННЯ НАНОКРИСТАЛІЧНИХ ПОКРИТТІВ ZrN, ОТРИМАНИХ ВАКУУМНО-ДУГОВИМ МЕТОДОМ НА НЕРЖАВІЮЧІЙ СТАЛІ AISI 430

*А.В.Таран, І.Є. Гаркуша, В.С. Таран, Р.М. Муратов, Т.С. Скобло, С.П. Романюк, В.В. Старіков, О.А. Батулин*

Нанокристалічні плівки нітриду цирконію були синтезовані вакуумно-дуговим методом із застосуванням високочастотного розряду (ВЧ) на поверхні нержавіючої сталі марки AISI 430 при 150 °С. Для вивчення фазового і хімічного складів, морфології поверхні, микроструктури і нанотвердості покриттів застосовувалися рентгенофлуоресцентний (XRF) та рентгеноструктурний (XRD) аналізи, скануюча електронна мікроскопія (SEM) з мікроаналізом (EDS) та просвічувальна електронна мікроскопія (TEM). Розроблена технологія забезпечує низькотемпературний синтез покриттів, зменшуючи утворення макрочастинок, а також дозволяє осаджувати покриття ZrN з твердістю 26,6...31,5 ГПа. Встановлено утворення однофазних полікристалічних плівок ZrN кубічної модифікації з розміром зерен 20 нм.